SHEAR TRANSFER MECHANISM OF PRE-CRACKED RC PLATES

Atsushi HABASAKI[1], Yoshio KITADA[2], Takao NISHIKAWA[3], Koichi MAEKAWA[4], Katsuhiko UMEKI[5], Mamoru YAMADA[6] And Kazunori KAMIMURA[7]

SUMMARY

This paper proposes a shear transfer model for cracked concrete based on test results, which can be applied to RC shear walls in nuclear power plant buildings that receive multi-directional loading. The test was performed using 12 pre-cracked RC plates which were loaded by shear force under constant axial stress.

In the proposed model, the reduction factor for shear stiffness is varied depending on the shear strain and normal strain of the crack fracture surface. It was confirmed that the test results can be simulated better by introducing the proposed equation into the FEM program than by using a specified reduction factor for shear stiffness (i.e., 0.8 or 0.125). The proposed model enables a more detailed assessment of the elasto-plastic behavior of RC shear walls of nuclear power plant buildings.

INTRODUCTION

In the current seismic design of nuclear power plant (NPP) buildings in Japan, seismic design loads in two orthogonal, horizontal directions are determined independently by seismic response analyses, whereas actual earthquake motion strikes NPP buildings in all three directions simultaneously. In order to clarify the effect of multi-directional loading on reinforced concrete (RC) seismic shear walls which are main earthquake-resistance element in NPP buildings, Nuclear Power Engineering Corporation (NUPEC) has been conducting a project entitled "Model Test of Multi-Axis Loading on RC Shear Walls". The objectives are to clarify the effects of multi-directional input forces on the ultimate strength of an RC seismic shear wall, and to predict nonlinear behavior of an RC seismic shear wall under multi-directional loading.

Seismic shear walls in an NPP building are loaded by both axial and shear forces repeatedly during an earthquake. Horizontal tensile cracks are generated by the axial force at the flange portion, and shear cracks are generated by the shear forces at the web portion. The prediction of nonlinear behavior of an RC shear wall with those cracks, especially the shear transfer mechanism at the crack fracture surface, is very important in NPP building design. Nevertheless, studies related to this point of view are limited in number. The main purposes of the present study are to develop a new shear transfer model for an RC shear wall with cracks and to improve the methodology of NPP seismic safety analysis relevant to multi-directional input motions.

SUMMARY OF TEST RESULTS

Cracks in RC shear walls under multi-directional loading are generated by the following process. First, horizontal cracks are generated by the out-of-plane moment of the motion applied perpendicular to the wall.

[1] *Seismic Engineering Center, Nuclear Power Engineering Corporation.*
[2] *Seismic Engineering Center, Nuclear Power Engineering Corporation.*
[3] *Department of Architecture, Tokyo Metropolitan Univ.*
[4] *Department of Civil Engineering, The Univ. of Tokyo.*
[5] *Nuclear Facilities Division, Obayashi Corporation*
[6] *Structural Engineering Department, Technical Research Institute, Obayashi Corporation*
[7] *Structural Engineering Department, Technical Research Institute, Obayashi Corporation Email:yamada@tri.obayashi.co.jp*

Shear cracks are then generated by the in-plane shear force of the motion applied in the orthogonal direction. The test was carried out as shown in Fig. 1 to produce the stress conditions of multi-axis loading by applying uni-axial stress with in-plane shear force to RC plates with horizontal cracks. Table 1 shows a summary of the

test results. Details of the test procedure are described in Ref.[2]. The following technical findings were obtained from the test results.

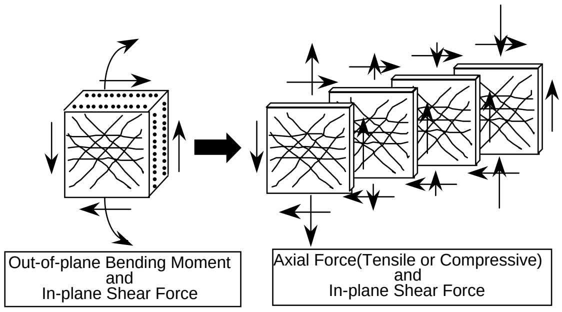

Fig.1 Basic Concept of Loading on the Specimens

(1) Initial shear stiffness is strongly dependent on the axial stress load. The values are larger for axial tension cases than for axial compression cases.
(2) The smallest reduction ratio for shear stiffness G_i/G_0 was 17% for D16+3.0. The largest reduction ratio was 84% for D13-1.5.
(3) The value of G_i/G_0 for the specimen without axial stress is about 50%.

Table.1 Test Results

Specimes Name	Horizontal Tencil Crack				Shear Crack			Rebar Yield			Max. Shear Stress			${}_iG$ (GPa)	G_0 (GPa)	${}_iG/G_0$ (%)
	${}_n\sigma_c$ (MPa)	${}_cf_t$ (MPa)	${}_n\sigma_c/{}_cf_t$	${}_n\varepsilon_c$ (μ)	τ_c (MPa)	$\tau_c/{}_cf_t$	γ_c (μ)	τ_y (MPa)	$\tau_y/(P_w ¥ {}_s\sigma_y)$	γ_y (μ)	τ_u (MPa)	$\tau_u/(P_w ¥ {}_s\sigma_y)$	γ_u (μ)			
D13+1.5	1.87	1.77	1.06	118	1.23	0.69	504	2.16	0.72	1990	3.90	1.31	17500	2.71	8.86	31
D13+0.0	1.67	1.54	1.08	87	1.72	1.12	648	3.12	1.05	3010	4.53	1.52	23400	5.09	9.31	55
D13-1.5	1.33	1.26	1.06	52	1.95	1.55	280	4.16	1.39	4000	5.08	1.70	20000	7.61	9.04	84
D16+3.0	1.61	1.33	1.21	144	1.24	0.93	1010	2.88	0.59	3010	4.94	1.00	20000	1.57	9.34	17
D16+1.5	1.48	1.14	1.30	146	1.24	1.09	474	4.47	0.91	4000	6.08	1.24	20100	3.77	10.56	36
D16+0.75	1.29	1.16	1.11	61	1.45	1.25	383	4.72	0.96	4000	6.34	1.29	18100	5.03	9.93	51
D16+0.0	1.39	1.19	1.17	86	1.58	1.33	430	5.11	1.04	4000	6.49	1.32	14500	5.60	9.55	59
D16-1.5	1.53	1.41	1.09	56	1.98	1.40	462	5.47	1.11	4000	7.31	1.48	13100	6.08	10.64	57
D16-3.0	1.41	1.32	1.07	40	1.93	1.46	392	6.20	1.26	4030	7.52	1.52	11000	6.52	10.38	63
D22+1.5	1.46	1.14	1.28	67	1.48	1.30	345	—	—	—	8.16	0.85	5030	5.26	11.23	47
D22+0.0	1.47	1.15	1.28	71	2.03	1.77	498	—	—	—	8.74	0.91	4830	5.57	11.50	48
D22-1.5	1.66	1.21	1.37	98	2.19	1.81	433	—	—	—	9.34	0.97	5010	7.54	11.41	66

${}_n\sigma_c$:Axial Stress for Horizontal Cracking
${}_n\varepsilon_c$:Axial Strain for Horizontal Cracking
τ_c :Shear Stress for Shear Cracking
γ_c :Shear Strrain for Shear Cracking
${}_cf_t$:Tensile Strength of Concrete in Specimens
τ_y :Shear Stress for Rebar Yielding
γ_y :Shear Strain for Rebar Yielding
τ_u :Max. Shear Stress
γ_u :Max. Shear Strain at τ_u
$G_0 = {}_cE/2(1+\nu)$ ${}_cE$:Young's Modulus
${}_iG$:Initial Shear Stiffness
σ_B :Concrete Strength
P_w:Rebar Ratio
${}_s\sigma_y$:Rebar Yield Stress
ν:Poisson's Ratio

Based on these findings, we conclude that FEM analysis of RC shear walls subjected to multi-directional loading does not allow adequate modeling with a uniform shear stiffness reduction factor for cracked concrete elements. Therefore, it is considered that the application of an appropriate shear transfer model of cracked concrete is required.

SHEAR TRANSFER MODEL OF CRACKED CONCRETE

Evaluation and Review of the Test Results

Figure 3 shows an overview of the evaluation and review of the test results. The envelope curve of the τ–γ relationship is based on the τ–γ relationship obtained by the test. The tangential shear stiffness G_i shown in the figure is obtained by the following equation ;

$$G_i = \Delta\tau_i / \Delta\gamma_I \qquad (1)$$

where, $\Delta\tau_i$: range of shear stress
$\Delta\gamma_i$: range of shear strain.

Before shear cracks are generated in a specimen,

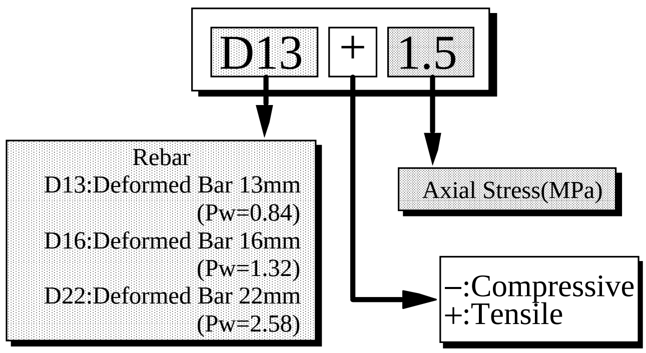

Fig. 2 Test Specimen Names

the following relationships can be determined ;

$\gamma_{cr} = \gamma_i$ (2)

$\varepsilon_{cr} = \varepsilon_i$ (3)

γ_{cr} : Shear strain in the crack direction
γ_i : Shear strain
ε_{cr} : Normal strain to the crack
ε_i : Axial strain

In other words, the shear stiffness at the crack fracture surface can be expressed as follows :

$$G_{cr} = G_i = \Delta\tau_i / \Delta\gamma_i \quad (4)$$

where, G_{cr} : Tangent shear stiffness at crack fracture surface

However, the data scatters widely when tangential shear stiffness G_i is calculated at each measured step. Thus, the G_i value is obtained after averaging and smoothing the τ–γ envelope curve using every third measurement.

Figure 4 shows the relationship between the tangential shear stiffness G_i of the τ–γ envelope and axial strain ε_i. Those data are taken from the data of all specimens before the shear cracks occurred. The vertical axis is normalized with the elastic shear modulus G_o. The elastic shear modulus G_o was obtained using Young's modulus and Poisson's ratio of concrete, which were obtained from the material test on each test specimen.

$$G_0 = E / \{2(1 + \nu)\} \quad (5)$$

where, ${}_cE$: Young's modulus obtained by material test
ν : Poisson's ratio of concrete obtained by material test

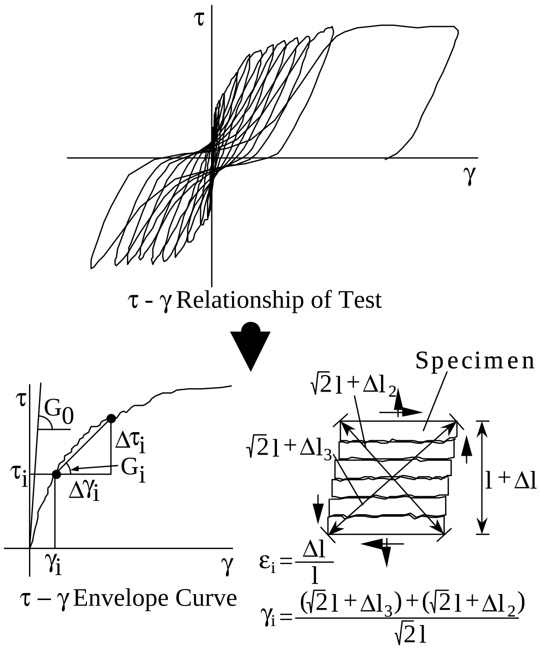

Fig. 3 Evaluation and Review

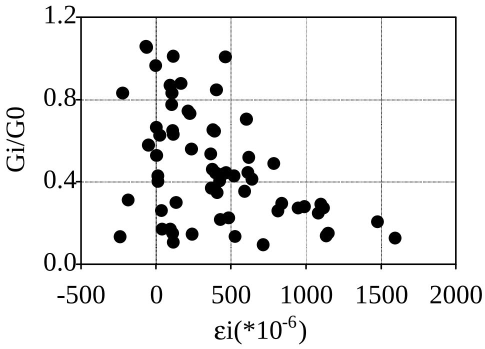

Fig. 4 G_i/G_0-ε_i (All Specimens)

The figure shows that the larger the value of ε_i, the smaller the maximum value of G_i/G_o.

The data in Fig. 4 are rearranged in light of the test parameters (reinforcement ratio and axial stress). The results are shown in Fig. 5 for reinforcement ratio and in Fig. 6 for axial stress. From these figures, the following findings were extracted :

(a) The larger the steel diameter, the smaller the axial strain
(b) The larger the tensile axial stress, the larger the axial stress in connection with the same steel-ratio test specimen
(c) There are cases where the axial strain of ε_i becomes negative value on the compressive side.

Values for ε_i were obtained in the range -250μ to 1600μ with the greater part of the data is obtained in the range –100μ to 700μ. The range is smaller than other experiments done in the past (the values obtained by Naganuma were in the range 500μ to 800μ [3]). However the actual axial strain is also considered small because the test parameters, i.e. the reinforcement ratio and axial stress are determined based on the results of a survey of the design conditions of actual NPP structures in Japan.
Figure 7 shows the relationships between tangential shear stiffness G_i and shear strain γ_i for the τ–γ curve envelope. The data are taken from the data for all specimens before shear cracks occurred. As can be seen in the figure, the values for γ_i were obtained in the range 0μ to 800μ, and the values for G_i/G_o depended largely on γ_i in this range. The data in Fig. 7 were rearranged in the same manner as the rearrangement of the data in Fig.4 regarding the test parameters for the reinforcement of the ratio and the axial stress. The results are shown in Fig.8 for the reinforcement ratio and in Fig. 9 for the axial stress.

Derivation of Proposed Model

Figure 10 shows the all G_i/G_o values evaluated by the test data displayed on a 3-D space composed of G_i/G_o , ε_i and γ_i axes. The test results show that G_i/G_o values form a certain curved surface in Fig. 10, and shear stiffness G_i at cracked fracture surfaces can be expressed as a function of ε_i and γ_i as :

$$G_i / G_0 = f(\varepsilon_i, \gamma_i) \qquad (6).$$

In order to find a function, that can express the tendency in Fig. 10 properly, we postulate the following function and do multiple regression analysis as follows:

$$G_i / G_0 = \frac{A}{\sqrt{\gamma_i^{\,2} + B \cdot \varepsilon_i^{\,2}}} \qquad (7)$$

where, A and B are treated as unknown fitting parameters.

The multiple regression analysis was done by replacing the negative value of ε_i with 0 by assuming that the cracks for this case were closed and the concrete was slightly deformed by elastic compression.

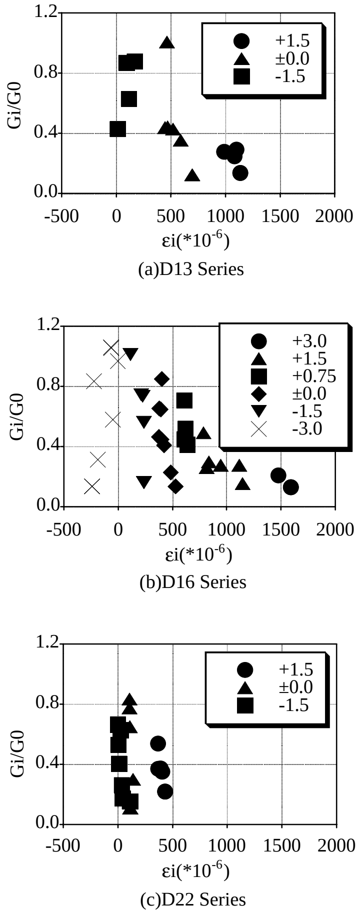

Fig. 5 G_i/G_0-ε_i (Categorized by Reinforcement Ratio)

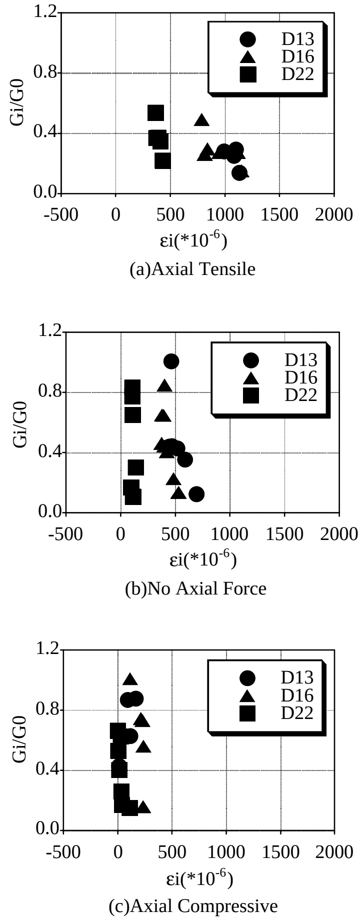

Fig. 6 G_i/G_0-ε_i relationship (Categorized by Axial Stress)

As a result, we find the following equation:

$$G_i / G_0 = \frac{85}{\sqrt{\gamma_i^{\,2} + 0.06\varepsilon_i^{\,2}}} \qquad (8)$$

Eq. (8) fits the test data fairly well because the value of the correlation coefficient obtained in the regression analysis is 0.777.

The outline of Eq.(8) is shown in Fig. 11 on the 3D space of $G_i/G_o - \varepsilon_i - \gamma_i$. Because Eq. (7) exceeds the value of 1.0 when both γ_i and ε_i are small, 1.0 is deemed the upper limit of G_i/G_o in the engineering judgement.

Thus, the shear transfer model for cracked concrete is defined as follows:

$$G_{cr} = \frac{85 \cdot G_0}{\sqrt{\gamma_{cr}^{\,2} + 0.06\varepsilon_{cr}^{\,2}}} \qquad (9)$$

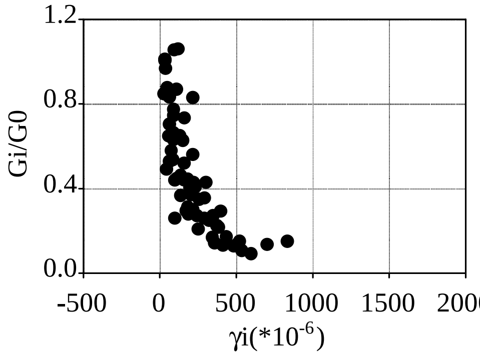

Fig. 7 Relationship of G_i/G_0-γ_i (All Specimens)

where, G_{cr} :Tangential shear stiffness at crack surface
G_o :Elastic shear modulus
γ_{cr} :Shear strain in crack direction

ε_{cr} :Normal strain on the crack

$G_{cr} \leq 1.0 \times G_o$,

$\varepsilon_{cr} = 0$ in the case of $\varepsilon_{cr} < 0$,

Figures 12 through 14 demonstrate the fitness of Eq. (9) to the test results. In this demonstration, the 3-D data obtained by superimposing Figs. 10 and 11 are cut into several pieces on the axis of one parameter to display the fitness in a plane of the two other parameter axes. Figures 12, 13 and 14 show the fitness in the planes of $G_i/G_o - \varepsilon_I$, $G_i/G_o - \gamma_i$ and $\varepsilon_i - \gamma_i$ respectively. Each of the figure shows the fitness for four typical ranges of the cut parameter. As can be seen in these figures, the tendency toward stiffness reduction observed in the test data is reasonably well expressed by Eq. (9).

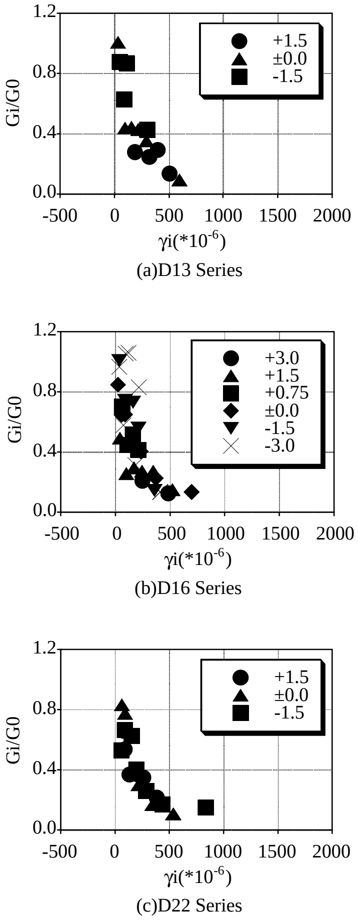

Fig.8 G_i/G_0-γ_i Relashionship (Categorized by Reinforcement Ratio)

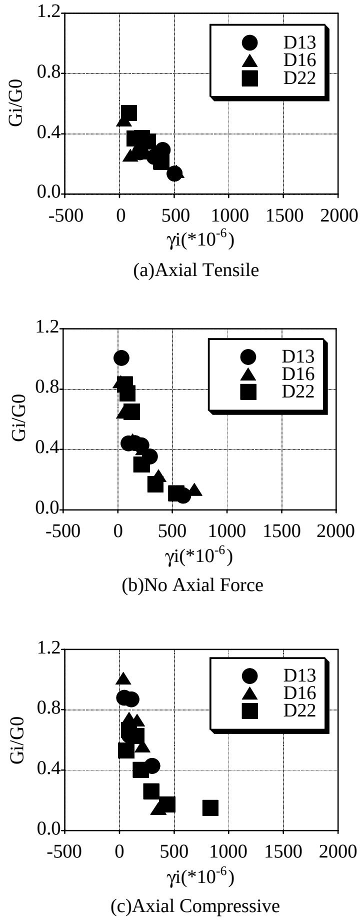

Fig. 9 G_i/G_0-γ_i Relashionship (Categorized by Axial Stress)

APPLICABILITY OF THE PROPOSED MODEL

Comparison with Existing Models

The proposed model was compared to existing models using the present test data. Three existing models were examined, the models proposed by Yamada and Aoyagi [4], Al-Mahidi [1], and Naganuma [3].

Figures 15 through 18 show the ratios of calculated shear stiffness to those evaluated from test data. In each figure, part (a) shows the influence of ε_i and part (b) shows that of γ_i. Both in the Yamada-Aoyagi model (Fig. 15) and the Al-Mahaidi model (Fig. 16), the ratios are calculated for secant shear stiffness. On the other hand, in Naganuma's model (Fig. 17) and the proposed model (Fig. 18), the ratios are calculated for tangential shear stiffness.

Calculated shear stiffness using the Yamada-Aoyagi model is in general larger than that of the test value. In particular, the calculated values tend to be significantly larger than the test values where the value of ε_i is larger than 500μ. Also, as the value of γ_i becomes larger, the calculated shear stiffness tend to exceed the test values. The reason could be that the horizontal cracks generated in the present test were a complicated with realistic pattern, while the Yamada-Aoyagi model is based on an experiment using an ideal crack. The calculated shear stiffness using the Al-Mahaidi model is smaller than the test value. The reason could be that the shear stiffness reduction factor in the Al-Mahaidi model is defined as 0.4 at the maximum of. The calculated shear stiffness by the Naganuma model tends to be smaller than the test value where γ_i is

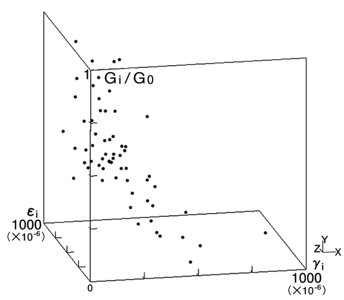

Fig.10 The Relationship of G_i/G_0-γ_i-ε_i

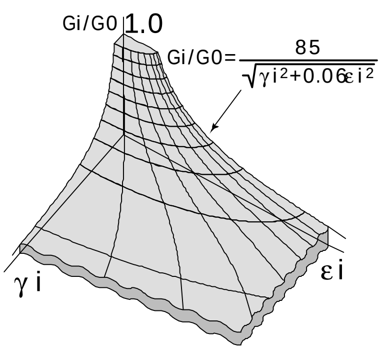

Fig. 11 Proposed Model

small (i.e., less than 200μ), whereas the value grows larger than the test value where γ_i is larger than 300μ. According to the Naganuma model, shear stiffness is relatively small at the beginning of crack generation and increases rapidly due to the interlocking phenomena of aggregates at the crack fracture surface. This behavior was not observed in the present test data. In addition, because few data at ε_{cr}< 500μ were obtained in the experiment from which the Naganum model is derived, the Naganuma model and the test do not show good agreement in this region.

On the other hand, shear stiffness calculated by the proposed model agrees well with the test values. Because the test parameters in the present test are based on a survey of actual NPP buildings in Japan, the proposed model is appropriate for the design analysis of NPP buildings.

Simulation Analysis by FEM

The test results were simulated using an FEM computer program which introduces the proposed model of shear transfer through tension cracks. For comparison, simulation analyses are performed using a shear stiffness reduction factor (hereafter referred to as β) of 0.125 and/or 0.80 as examples of analysis by the conventional method.

Figures 19 through 21 compare the τ - γ relationship obtained by simulation analysis and the test results. The comparison was performed by focusing on changes of the initial and the second slopes in a chart of the τ – γ relationship before and after shear crack generation. The test data and simulation results are compared first before the generation of the shear crack. The stiffness of all the simulation results obtained using the β value of 0.125 was smaller than that of the test results. The simulation results using the β value of 0.8 agree well with the test data for zero axial stress (Fig. 20) and for compressive axial stress (Fig. 21).

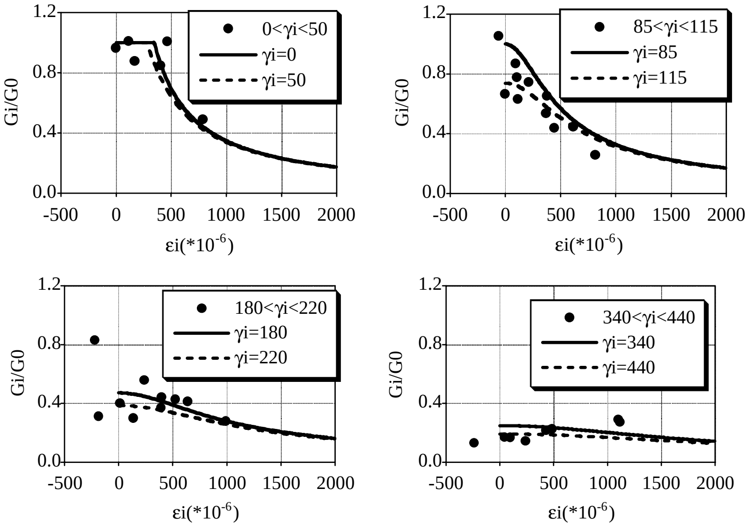

Fig. 12 Comparison of the Proposed Eq. and the Test Results (1)

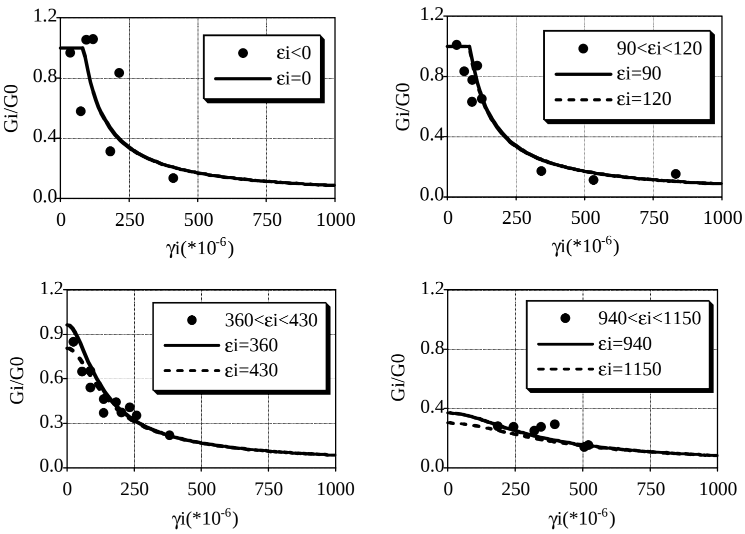

Fig. 13 Comparison of the Proposed Eq. and the Test Results (2)

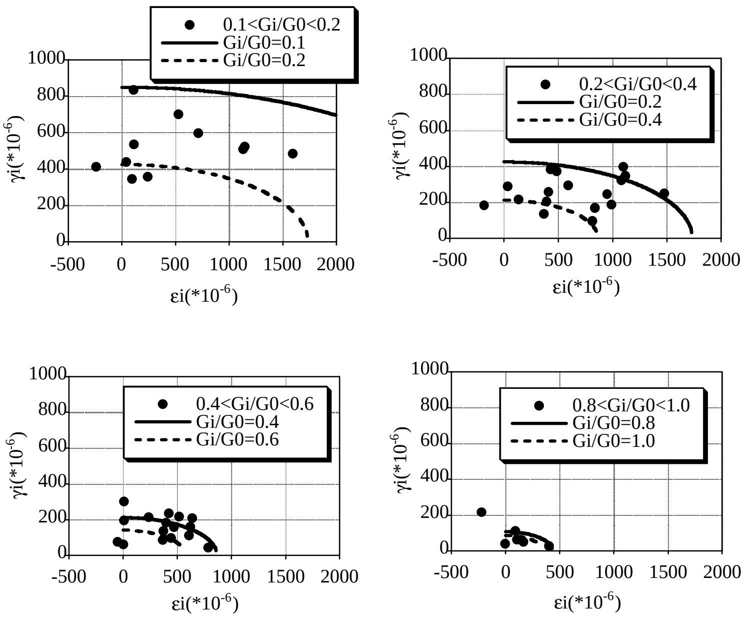

Fig. 14 Comparison of the Proposed Eq. and the Test Results (3)

However, the stiffness becomes larger for tensile axial stress (Fig. 19). All the simulation results using the proposed model fits better to the test data than the results using a shear stiffness reduction factor of 0.125 or 0.8. For the second slope after the shear crack generation, all of the results using the β value of 0.125 or 0.8 or the proposed model agree well with the test results. The test results were simulated well by introducing the proposed model into an FEM computer program.

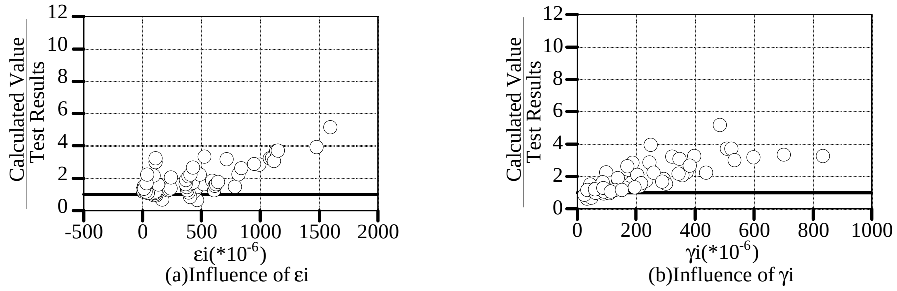

Fig. 15 Secant Shear Stiffness with the Yamada-Aoyagi Model and Authors' Test

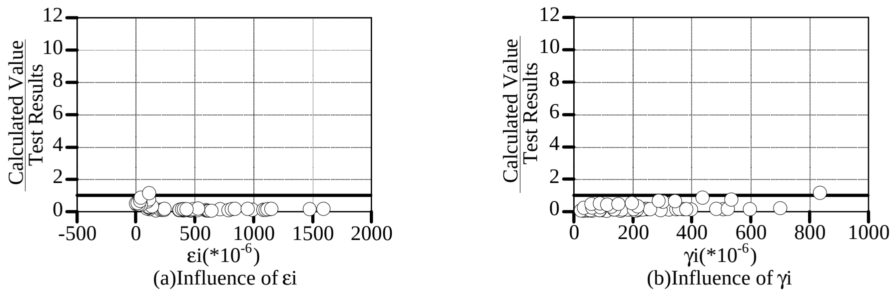

Fig. 16 Secant Shear Stiffness with the Al-Mahaidi Model and Authors' Test

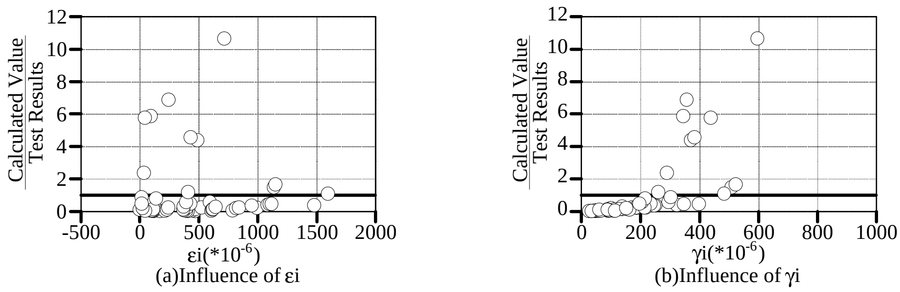

Fig. 17 Tangential Shear Stiffness with the Naganuma Model and Authors' Test

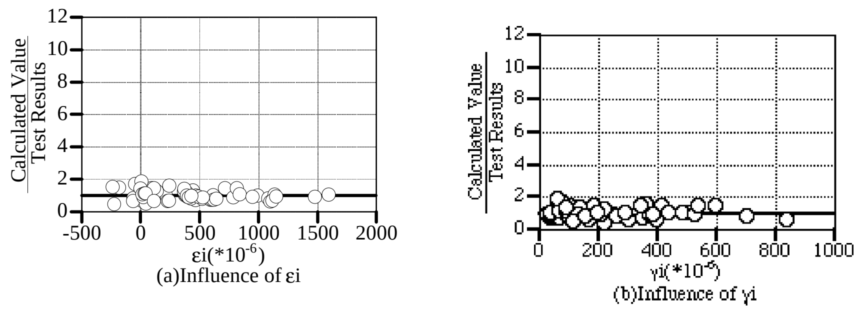

Fig. 18 Tangential Shear Stiffness with the Proposed Equation and Authors' Test

CONCLUSIONS

Tests were conducted on 12 pre-cracked RC plates by loading shear force under constant axial stress. Using this test data, a shear transfer model of tension cracks was proposed based on the test results. The model is applicable to RC shear walls under multi-directional loading. The applicability of the proposed shear transfer model was examined using the test results. Major outcomes of the present study include :

(1) A shear transfer model for cracked concrete was proposed based on test results of 12 specimens. In the proposed model, the shear stiffness reduction factor was varied depending on shear strain and normal strain on the crack fracture surface.

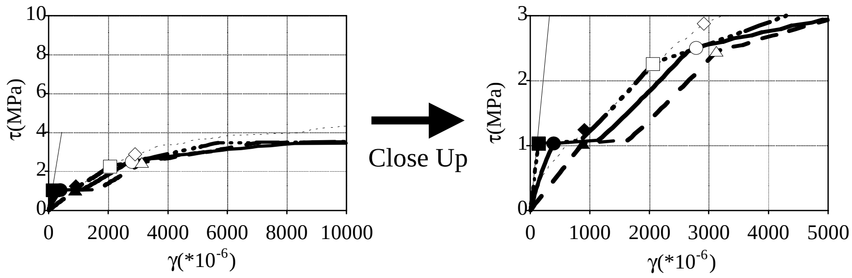

(a) General View (b) Close up View

Fig. 19 Simulation Results (D16+3.0)

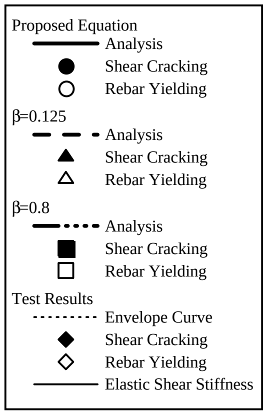

Legend of Figs. 19~21

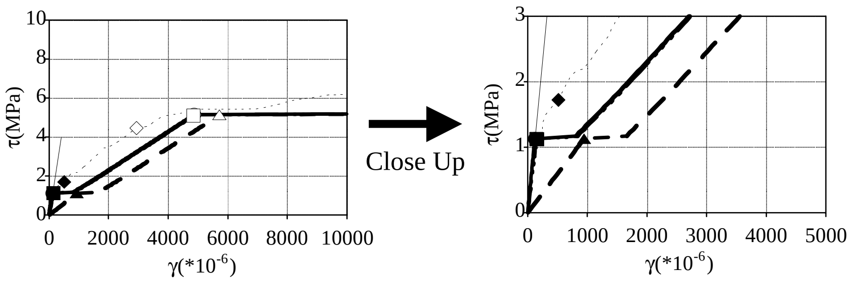

(a) General View (b) Close up View

Fig. 20 Simulation Results (D16+0.0)

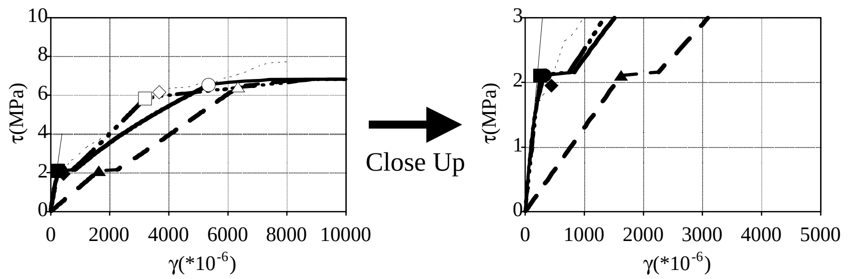

(a) General View (b) Close up View

Fig. 21 Simulation Results (D16-3.0)

(2) It was confirmed that the test results are simulated better by introducing the proposed model into an FEM program than by using a specified reduction factor for shear stiffness (i.e., 0.8 or 0.125). The proposed model enables detailed assessment of the elasto-plastic behavior of RC shear walls after strength reduction due to tension cracks in the wall.

ACKNOWLEDGMENTS

This work was performed by NUPEC under commission by the Ministry of International Trade and Industry (MITI) Japan. Technical issues have been discussed in the Advisory Committee on the Model Tests of Multi-axis Loading on RC Shear Walls established within NUPEC (Chairperson; Dr.T.Nishikawa). The authors wish to express their thanks to all the members of committee for their valuable suggestions and cooperation.

REFERENCES

1. Al-Mahidi R.S.H., *"Nonlinear FEM analysis of RC deep members"*, Report 79-1, Department of Structural Engineering, Cornell University, 1979.
2. Kitada, Y., et al., *"Shear Behavior of Pre-cracked RC Plates Subjected to Combined Axial and Shear Stress"*, to be published in Proc. SMiRT-15, Div. H, H08-2, Aug.1999, Seoul.
3. Naganuma K., *"Nonlinear analytical model for RC panels under in-plane stresses"*, Journal of Structural and Construction Engineering, Architectural Institute of Japan, No.421, pp39-48, Mar., 1991.
4. Yamada K. and Aoyagi Y., *"Shear transfer across cracks"*, Proceedings of JCI 2nd colloquium on shear analysis of RC structures, Japan Concrete Institute, pp19-28, Oct., 1983.